

Realization of robust Ohmic contact for semiconducting black arsenic by coupling with graphene

Xinjuan Cheng(程新娟) and Xuechao Zhai(翟学超)†

Citation: Chin. Phys. B, 2025, 34 (**2**): 027402. DOI: 10.1088/1674-1056/ada0b3
Journal homepage: http://cpb.iphy.ac.cn; http://iopscience.iop.org/cpb

What follows is a list of articles you may be interested in

Moiré superlattices arising from growth induced by screw dislocations in layered materials

Fuyu Tian(田伏钰), Muhammad Faizan, Xin He(贺欣), Yuanhui Sun(孙远慧), and Lijun Zhang(张立军)
Chin. Phys. B, 2024, 33 (**7**): 077403. DOI: 10.1088/1674-1056/ad4cdc

Customizing topological phases in the twisted bilayer superconductors with even-parity pairings

Conghao Lin(林丛豪), Chuanshuai Huang(黄传帅), and Xiancong Lu(卢仙聪)
Chin. Phys. B, 2023, 32 (**8**): 087401. DOI: 10.1088/1674-1056/acd3e3

Device physics and design of FD-SOI JLFET with step-gate-oxide structure to suppress GIDL effect

Bin Wang(王斌), Xin-Long Shi(史鑫龙), Yun-Feng Zhang(张云峰), Yi Chen(陈伊), Hui-Yong Hu(胡辉勇), and Li-Ming Wang(王利明)
Chin. Phys. B, 2021, 30 (**4**): 047401. DOI: 10.1088/1674-1056/abd2a2

Simulation study of device physics and design of GeOI TFET with PNN structure and buried layer for high performance

Bin Wang(王斌)†, Sheng Hu(胡晟), Yue Feng(冯越), Peng Li(李鹏), Hui-Yong Hu(胡辉勇), and Bin Shu(舒斌)
Chin. Phys. B, 2020, 29 (**10**): 107401. DOI: 10.1088/1674-1056/ab99b5

Enhancement of off-state characteristics in junctionless field effect transistor using a field plate

Bin Wang(王斌), He-Ming Zhang(张鹤鸣), Hui-Yong Hu(胡辉勇), Xiao-Wei Shi(史小卫)
Chin. Phys. B, 2018, 27 (**6**): 067402. DOI: 10.1088/1674-1056/27/6/067402

Realization of robust Ohmic contact for semiconducting black arsenic by coupling with graphene

Xinjuan Cheng(程新娟) and Xuechao Zhai(翟学超)†

Department of Applied Physics, and MIIT Key Laboratory of Semiconductor Microstructures and Quantum Sensing, Nanjing University of Science and Technology, Nanjing 210094, *China*

(Received 31 October 2024; revised manuscript received 6 December 2024; accepted manuscript online 18 December 2024)

Ohmic contacts are fundamental components in semiconductor technology, facilitating efficient electrical connection and excellent device performance. We employ first-principles calculations to show that semimetallic graphene is a natural Ohmic contact partner of monolayer semiconducting black arsenic (BAs), for which the top of the valence band is below the Fermi energy of the order of 10^2 meV. The Ohmic contact arises from the giant Stark effect induced by van der Waals electron transfer from BAs to graphene, which does not destroy their respective band features. Remarkably, we show that this intrinsic Ohmic contact remains robust across a wide range of interlayer distances (adjustable by strain) or vertical electric fields, whereas the weak spin splitting of the order of 1 meV induced by symmetry breaking plays little part in Ohmic contact. These findings reveal the potential applications of graphene–BAs in ultralow dissipation transistors.

Keywords: semiconductor technology, Ohmic contact, heterobilayer, Stark effect

PACS: 74.78.Fk, 61.82.Fk, 32.60.+i

DOI: 10.1088/1674-1056/ada0b3 **CSTR:** 32038.14.CPB.ada0b3

1. Introduction

In semiconductor technology, low-resistance Ohmic contacts are fundamental components in facilitating efficient electrical connection, enhancing device performance and supporting higher scalability and integration.[1] High-quality Ohmic contacts minimize power loss and heat generation, thereby improving device efficiency and reliability, and also contribute to the speed and stability of device operation.[2,3] As semiconductor technology advances towards smaller feature sizes and increased integration density,[4,5] the significance of high-quality Ohmic contacts becomes even more pronounced. To ensure low resistance and compatibility with the device's overall design, identification of better Ohmic contact partner(s) for a desired semiconductor has always been a key challenge.[2–10]

Two-dimensional (2D) black arsenic (BAs), one of the best 2D semiconductors prepared in recent years,[11–13] has a unique puckered orthorhombic structure similar to that of black phosphorus.[14] It offers notable advantages over 2D transition metal dichalcogenides (TMDs) in terms of relative thermal stability and mechanical flexibility,[15] a highly tunable bandgap (from 0.3 eV to 1.5 eV) by changing the thickness[16,17] or strain,[18,19] larger carrier mobility (reaching the order of 10^2–10^3 $\mathrm{cm}^2 \cdot \mathrm{V}^{-1} \cdot \mathrm{s}^{-1}$)[16,20] and extreme in-plane anisotropy.[20–23] These attributes make 2D BAs a highly promising material for next-generation semiconductor devices. A natural question arises: how can we achieve an ideal Ohmic contact in 2D BAs-based devices?

The conventional approach of directly depositing metal electrodes on arbitrary 2D semiconductors is challenging for producing a desired Ohmic contact, as it inevitably disrupts the covalent bonds within the atomic lattice and introduces defects.[2–5] To achieve Ohmic contacts for 2D semiconductors, van der Waals (vdW) engineering[24] provides a feasible strategy that can be incorporated into the existing process technologies, typically metallic NbS_2[27,28] or semimetallic bismuth[29] as vdW Ohmic partners of suitable semiconducting TMDs. Nevertheless, the most active 2D semiconductors that form high-resistance Schottky contacts with graphene (a star material of this century[31,32]) are the norm; these include TMDs,[29] black phosphorus,[30] phosphorene[31,32] and Janus materials.[33–36] Even if Ohmic contacts are possible, they often require stringent conditions such as a large gate voltage[33] or precise adjustment of the interlayer distance.[34–36] To date, vdW heterobilayers constructed from graphene and elemental semiconducting BAs have yet to be explored.

Here, we perform first-principles calculations for a graphene–BAs heterobilayer and intriguingly, find that it is a promising Ohmic contact in its natural most stable state without fine tuning of gate voltage and atomic adjustment as previously done.[33–36] This Ohmic contact arises from a giant Stark effect[17,37] (band shifts), for which the driving interlayer electric field is induced by vdW electron transfer from BAs to graphene, while the heterobilayer inherits the basic band features from both parents because the vdW coupling is weak.[29–36] Importantly, we demonstrate that the Ohmic contact remains robust against variations of interlayer distance (adjustable via strain) and perpendicular electric field across a

†Corresponding author. E-mail: zhaixuechao@njust.edu.cn

© 2025 Chinese Physical Society and IOP Publishing Ltd. All rights, including for text and data mining, AI training, and similar technologies, are reserved.

wide range of parameters. In contrast, Schottky contacts only manifest when the electric field along the direction of the intrinsic interlayer dipole moment exceeds 0.8 V·nm^{-1}.

Compared with the existing theoretical predictions in graphene–complex compound semiconductors,[38–45] the graphene–BAs heterobilayer here has a more robust Ohmic contact performance because the valence band top is about 0.25 eV below the Fermi energy (large enough to make it strong against disturbance) in addition to its natural advantages in terms of single-element composition and relatively easy experimental preparation. Additionally, we show that spin splitting of the order of 1 meV arising from the interface-induced symmetry breaking plays little role in Ohmic contact. These findings underscore the potential applications of graphene–BAs in 2D chip integrated circuits.

2. Results and discussion

We employ the standard density functional theory (DFT) as implemented in the Vienna *ab initio* Simulation Package to perform calculations, including spin–orbit coupling in all calculations.[46] We describe the electron–ion interaction with projector-augmented-wave potentials, treat the electronic exchange–correlation functional using the Perdew–Burke–Ernzerhof (PBE) generalized gradient approximation,[47] and use the dispersion-corrected DFT method to describe the vdW interaction.[48] The energy cutoff is fixed at 500 eV. An off-plane vacuum space of 20 Å is applied to avoid the effects of a periodic boundary. Atomic positions are fully relaxed until the maximum force on each atom is less than 10^{-3} eV·Å^{-1}. The energy convergence threshold is set to 10^{-6} eV. The calculations are performed using an $8\times5\times1$ Monkhorst–Pack k-point mesh. The dipole correction is employed to set the electric field in the vacuum region to zero.[49] The Fermi energy ($E=0$ in the band structure) is automatically determined by self-consistent calculations.

Firstly, we examine the geometrical and electronic characteristics of the individual BAs monolayer in Fig. 1(a) and the single-layer graphene in Fig. 1(b). Single-layer BAs has an orthorhombic structure with space group *Pmna*, and graphene has a hexagonal lattice with a space group $P6/mmm$. Both BAs and graphene have inversion symmetry. Pristine graphene has an optimized lattice constant of 2.457 Å and is a semimetal with zero bandgap, while the BAs monolayer has an optimized lattice constant of 3.650 Å and an indirect bandgap of 0.81 eV, basically consistent with the values in the literature.[16,18] Both graphene and BAs possess two main crystal directions, armchair (x) and zigzag (y). For all the possible graphene–BAs heterobilayers, the most symmetrical stacking (higher symmetry often relates to a more stable energy-favorable configuration) is to align the zigzag orientations of graphene and BAs exactly, similar to that in graphene–black phosphorus[30] and graphene–phosphorene[50] which have the same type of heterostructure. To determine the most stable configuration, we perform the following calculations. In Fig. 1(c), we calculate the binding energy $E_{\rm b}$ versus the interlayer distance d with the relation

$$E_{\rm b}=E_{\rm graphene-BAs}-E_{\rm graphene}-E_{\rm BAs}. \tag{1}$$

Here, $E_{\rm graphene-BAs}$, $E_{\rm graphene}$ and $E_{\rm BAs}$ indicate the total energy of the heterostructure, graphene and BAs, respectively. The optimized interlayer distance between graphene and BAs is $d_0=3.62$ Å, which is taken as the initial state in Fig. 1(d) to plot the dependence of $E_{\rm graphene-BAs}$ on interlayer slipping $(\Delta x,\Delta y)$. Our results indicate that the energy variation is not that sensitive to Δy, whereas the initial state is indeed the lowest-energy state.

Secondly, we show the electronic properties of graphene–BAs in Fig. 1(e) to determine whether the heterobilayer is an Ohmic contact or a Schottky contact. The interfacial contact properties can be accurately determined using the Schottky–Mott rule[12,51,52] to ascertain the Schottky barrier height (SBH) as

$$\Phi_{\rm n}=E_{\rm CBM}-E_{\rm F},\quad \Phi_{\rm p}=E_{\rm F}-E_{\rm VBM}. \tag{2}$$

Here, $\Phi_{\rm n}$ and $\Phi_{\rm p}$ represent the SBH for electrons and holes, respectively, in the BAs layer, $E_{\rm VBM}$ and $E_{\rm CBM}$ denote the valence band maximum (VBM) and the conduction band minimum (CBM) for BAs, respectively, and $E_{\rm F}$ represents the Fermi energy of the heterobilayer. Obviously, the bandgap for the BAs layer is determined by $E_{\rm g}=\Phi_{\rm p}+\Phi_{\rm n}$. It is seen that $\Phi_{\rm n}>0$ holds here due to $E_{\rm CBM}>E_{\rm F}$ and $\Phi_{\rm p}<0$ is valid because the Fermi energy of the heterobilayer intersects the valence band of BAs. Therefore, the graphene–BAs heterobilayer is a naturally occurring Ohmic contact determined by the general relation $\mathrm{sgn}(\Phi_{\rm n}\Phi_{\rm p})\le 0$.[12] The layer-projected density of states is plotted on the right of Fig. 1(e), depicting the contributions near the Fermi energy, in agreement with the projected energy bands. Significantly, the top of the valence band is below the Fermi energy by 0.25 eV ($|\Phi_{\rm p}|$).

Next, it is necessary to clarify the mechanism of formation of the Ohmic contact in terms of vdW charge transfer. We calculate the charge density difference $\Delta\rho=\rho_{\rm graphene-BAs}-\rho_{\rm graphene}-\rho_{\rm BAs}$ in Fig. 2(a) and the corresponding electrostatic potential in Fig. 2(b). Evidently, there exists an accumulation of electrons within the graphene layer accompanied by a corresponding depletion in the BAs layer. The graphene layer exhibits a much deeper potential than the BAs layer [Fig. 2(b)], leading to a significant drop in interlayer potential, which can efficiently exert a facilitating charge injection in BAs-based logic circuits. As a result, the transfer of

electrons occurs predominantly from BAs to graphene, consistent with the band structure in Fig. 1(e). Estimated by the Bader analysis,[53] approximately 0.152 electron per unit cell is transferred by vdW coupling. This drives a strong interlayer electric dipole, resulting in a giant Stark effect as shown in Fig. 2(c). The fast response of E_{VBM} [dominated by the $4p_x$ orbit of As; see Fig. 1(e)] to the interfacial electric field reflects the unique advantages of BAs:[17] it is superior to other heterostructures without a strong interface-induced anisotropic Stark effect.[38–45]

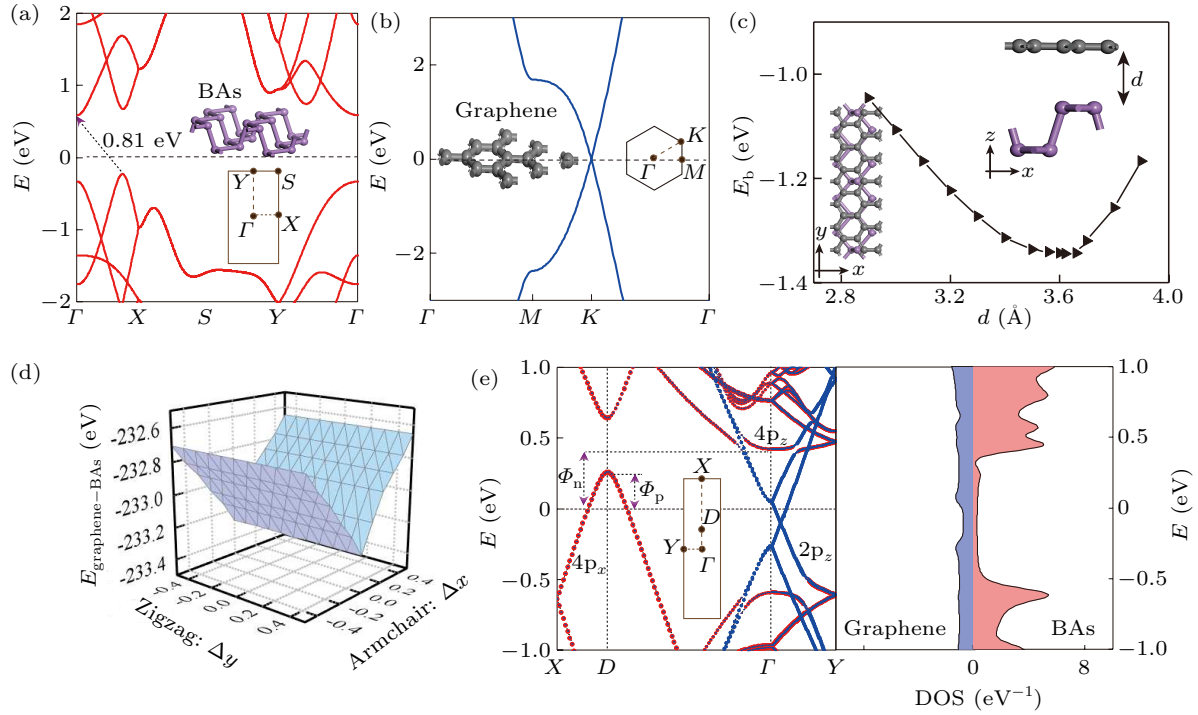


Fig. 1. [(a) and (b)] Band structures of monolayer BAs and graphene, respectively. (c) Dependence of binding energy on interlayer distance d for a graphene–BAs heterobilayer. To better optimize the lattice mismatch, a supercell is constructed from a combination of 1×6 graphene unit cells and 1×4 BAs unit cells aligned along the armchair direction. After optimization, the lattice constants are refined to $a=4.36$ Å and $b=14.68$ Å. The insets in (a)–(c) denote the real-space structures. (d) Total energy versus interlayer slipping (Δx, Δy) with respect to the lowest-energy state $d=3.62$ Å in (c). (e) Band structure and density of states (DOS) of graphene–BAs. The dominant orbitals $2p_z$ (C atom) and $4p_{x(z)}$ (As atom) are denoted. The corresponding Brillouin zones are plotted in the insets of panels (a), (b) and (e).

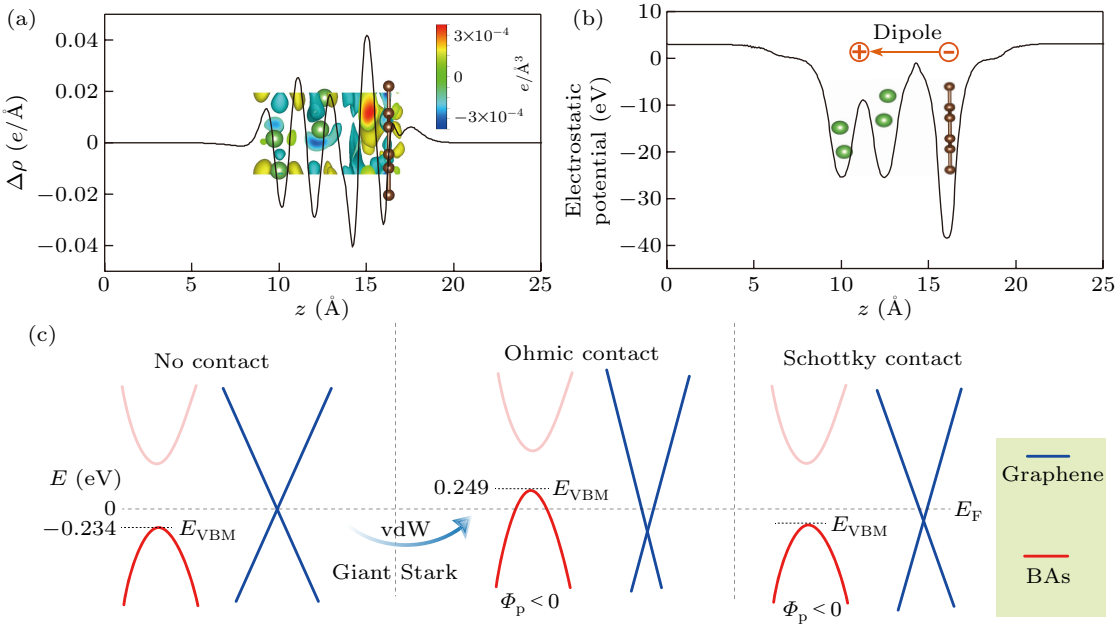


Fig. 2. [(a) and (b)] The calculated charge density difference (solid line) for graphene–BAs and the corresponding electrostatic potential in the z-direction, respectively. The color in panel (a) marks the isosurface of charge density difference in the atomic structure. The top inset in (b) qualitatively shows the interlayer electric dipole. (c) Band characteristics of no contact (left) extracted from Figs. 1(a) and 1(b), Ohmic contact (middle) plotted according to Fig. 1(e), and Schottky contact (right) only for comparison. The dashed lines in all the bands denote the Fermi energy. Due to $\Phi_{\mathrm{n}}>0$ always holding here, only Φ_{p} determined by Eq. (2) is denoted.

Now, we ask whether the Ohmic contact can withstand changes in the interlayer distance, since for actual experimental samples the Ohmic contact can inevitably be disturbed by the substrate or the environment. To answer this, we calculate the SBH as a function of the interlayer distance d in Fig. 3(a), with the definition $\Delta d = d - d_0$ ($d_0 = 3.62$ Å), where Δd is tunable by vertical strain in principle.[18] Our results indicate that $\Phi_n > 0$ always holds here. For $\Delta d < 0$, the band of BAs moves upwards and that of graphene moves downwards, leading to a better Ohmic contact (Φ_p reaches -0.362 eV for $\Delta d = -0.3$ Å). This is because the vdW coupling becomes stronger. For $\Delta d > 0$, the bands of each individual monolayer exhibit contrasting movements, eventually bringing the Dirac cone of graphene and the VBM of BAs to the same energy level ($\Phi_p \to 0$). For -0.3 Å $\leq \Delta d \leq 1.2$ Å that concerns us here, the Ohmic contact property is always valid. It was checked that the vdW coupling is weak enough to be ignored for $\Delta d \simeq 1.6$ Å when the interlayer distance is about 5.2 Å.

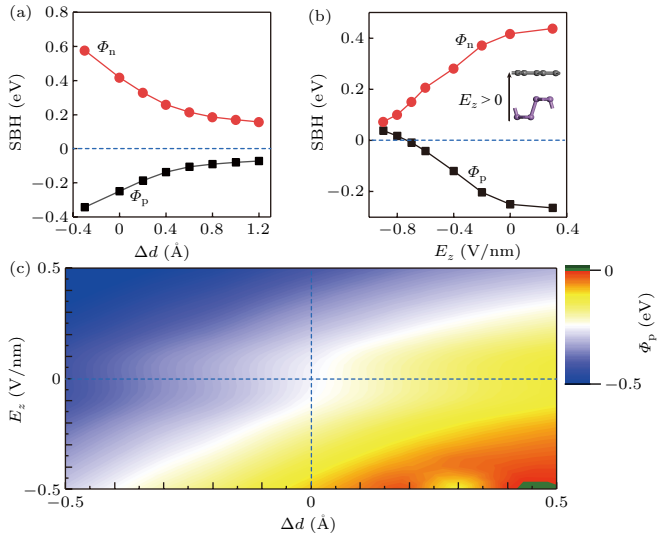


Fig. 3. Dependence of the Schottky barrier height (SBH) $\Phi_{n,p}$ on (a) the interlayer distance variation $\Delta d = d - d_0$ with respect to $d_0 = 3.62$ Å without external fields, (b) the vertical electric field E_z for $d_0 = 3.62$ Å and (c) the combined effect from Δd and E_z.

Moreover, we consider the influence of vertical electric field E_z on the Ohmic contact, which can be altered by the substrate or gate in a device. As is shown in Fig. 3(b), $\Phi_n > 0$ is not destroyed here. For $E_z > 0$, the VBM of the BAs layer moves upwards and the Dirac cone of the graphene layer moves downwards, leading to an increase in $|\Phi_p| = -\Phi_p$. Thus, a positive E_z helps to form a stronger Ohmic contact. For $E_z < 0$ [along the dipole direction in Fig. 2(b)], the Dirac bands of graphene move significantly upwards as $|E_z|$ increases, while the valence band of BAs shifts downwards (closer to the Fermi energy). When E_z reaches approximately -0.8 V·nm^{-1}, the VBM of the BAs layer and the Dirac cone of graphene meet at the Fermi energy and a critical point between Ohmic contact and Schottky contact appears. This means that the Ohmic contact is destroyed when a large $|E_z| = -E_z$ is applied. We further consider the combined effect of Δd and E_z in Fig. 3(c). This shows that the Ohmic contact is robust against the variations of $(E_z, \Delta d)$ in a wide range, except where both E_z for $E_z < 0$ and Δd are large enough (see the bottom right corner).

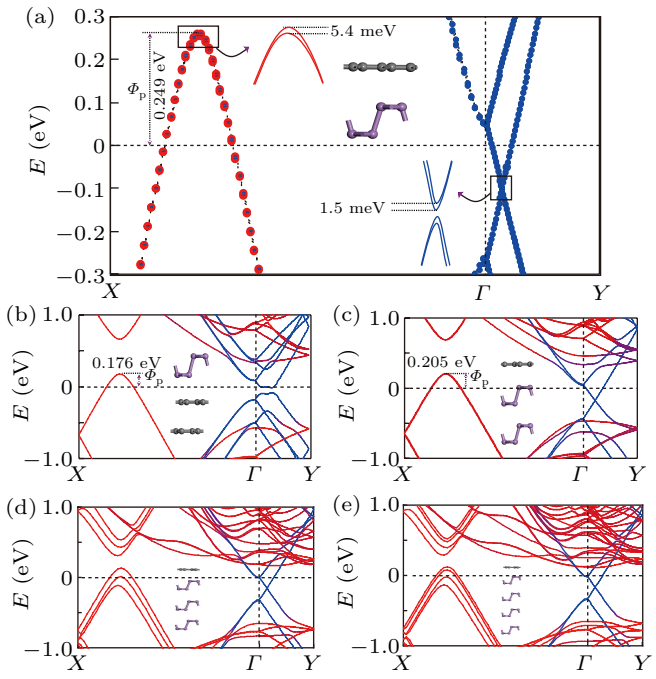


Fig. 4. (a) Influence of spin splitting on Ohmic contact for graphene–BAs as taken from the fine band structure in Fig. 1(e). The top (bottom) inset shows the band edges for BAs (graphene). (b)–(e) Band structures for BAs–bilayer graphene, graphene–bilayer BAs, graphene–trilayer BAs and graphene–four-layer BAs, respectively.

Finally, we discuss the influence of several factors on Ohmic contact. (i) The first factor is band spin splitting, which is inevitably induced by the breakage of interface symmetry. It is known that a single graphene layer has inversion symmetry, leading to no spin splitting in Fig. 1(b), likewise for a single BAs layer in Fig. 1(a). When graphene and BAs are vdW coupled, inversion symmetry is naturally broken. To distinguish symmetry breaking from band structure, we show the fine band structure in Fig. 4(a), which is obtained by narrowing the energy range in Fig. 1(e). It is seen that the spin splitting near the band edges is of the order of 1 meV, which is completely negligible compared with the Ohmic-contact Schottky potential $\Phi_p = -0.249$ eV in the regime of the PBE approximation, and does not change when we use the hybrid density functional method (HSE06) to perform calculations, in which the Ohmic contact parameter $\Phi_p = -50.3$ meV is obtained. Even when we tune $(E_z, \Delta d)$ in Fig. 3, the spin splitting cannot exceed 8 meV. Consequently, the Ohmic contact is insensitive to spin splitting for graphene–BAs despite symmetry breaking. (ii) The second factor is the number of layers. We perform calculations for BAs–bilayer graphene in Fig. 4(b) and graphene–bilayer BAs in Fig. 4(c), and also more layers in Figs. 4(d) and

4(e). It is shown that the valence band top of BAs is still below the Fermi energy of the order of 10^2 meV, reflecting the robustness of the excellent Ohmic contacts. (iii) The third factor is interlayer slipping in Fig. 1(d). Our further calculations indicate that the interlayer slipping $\Delta x = 0$ for $\Delta y \neq 0$ does not alter the property of Ohmic contact despite weak band variations.

3. Conclusion

In summary, we have shown that semimetallic graphene is the matching Ohmic contact partner of semiconducting BAs when formed to the vdW heterobilayer. This Ohmic contact originates from a giant Stark effect induced by vdW electron transfer from BAs to graphene, and most significantly is always valid when interlayer distance and vertical electric field vary over wider ranges. We have also shown that the Ohmic contact is basically unaffected by the weak spin splitting induced by symmetry breaking and is still robust against the increase in the number of heterostructure layers (in the case of a few layers). These results suggest that 2D BAs is promising for application in ultralow consumption semiconductor devices that use graphene as electrodes.

Acknowledgment

Project supported by the National Natural Science Foundation of China (Grant Nos. 62374088 and 12074193).

References

[1] Burghartz J N 2013 *Guide to State-of-the-Art Electron Devices* (Chichester: John Wiley & Sons Inc)
[2] Allain A, Kang J, Banerjee K and Kis A 2015 *Nat. Mater.* **14** 1195
[3] Schulman D S, Arnold A J and Das S 2018 *Chem. Soc. Rev.* **47** 3037
[4] Ni J, Fu Q, Ostrikov K, Gu X, Nan H and Xiao S 2022 *Nanotechnology* **33** 062005
[5] Peng B, Cao K, Lan A H Y, Chen M, Lu Y and Chan P K L 2020 *Adv. Mater.* **32** 2002281
[6] Gambino J P and Colgan E G 1998 *Mater. Chem. Phys.* **52** 99
[7] Liu Y, Guo J, Zhu E, Liao L, Lee S J, Ding M, Shakir I, Gambin V, Huang Y and Duan X 2018 *Nature* **557** 696
[8] Wang Y, Kim J C, Wu R J, Martinez J, Song X, Yang J, Zhao F, Mkhoyan A, Jeong H Y and Chhowalla M 2019 *Nature* **568** 70
[9] Xu S Y, Yu M, Yuan D, Peng B, Yuan L, Zhang Y M and Jia R X 2024 *Chin. Phys. B* **33** 017302
[10] Guo J, Zhu J, Liu S, Liu J, Xu J, Chen W, Zhou Y, Zhao X, Mi M and Yang M 2023 *Chin. Phys. B* **32** 037303
[11] Xiong Y, Xu D, Feng Y, Zhang G, Lin P and Chen X 2023 *Adv. Mater.* **35** 2206939
[12] Mohanta M K and Sarkar A D 2021 *Appl. Surf. Sci.* **540** 148389
[13] Shen P C, Su C, Lin Y, Chou A S, Cheng C C, Park J H, Chiu M H, Lu A Y, Tang H L, Tavakoli M M, Pitner G, Ji X, Cai Z, Mao N, Wang J, Tung V, Li J, Bokor J, Zettl A, Wu C I, Palacios T, Li L J and Kong J 2021 *Nature* **593** 211
[14] Xia F, Wang H, Hwang J C M, Castro Neto A H and Yang L 2019 *Nat. Rev. Phys.* **1** 306
[15] Du G, Ke F, Han W, Chen W B, Xia Q, Kang J and Chen Y 2023 *J. Phys. Chem. Lett.* **14** 8676
[16] Zhong M, Xia Q, Pan L, Liu Y, Chen Y, Deng H X, Li J and Wei Z 2018 *Adv. Funct. Mater.* **28** 1802581
[17] Sheng F, Hua C, Cheng M, Hu J, Sun X, Tao Q, Lu H, Lu Y, Zhong M, Watanabe K, Taniguchi T, Xia Q, Xu Z A and Zheng Y 2021 *Nature* **593** 56
[18] Kamal C and Ezawa M 2015 *Phys. Rev. B* **91** 085423
[19] Gao C, Li R, Zhong M, Wang R, Wang M, Lin C, Huabf L, Cheng Y and Huang W 2020 *J. Phys. Chem. Lett.* **11** 93
[20] Chen Y, Chen C, Kealhofer R, Liu H, Yuan Z, Jiang L, Suh J, Park J, Ko C, Choe H S, Avila J, Zhong M, Wei Z, Li J, Li S, Gao H, Liu Y, Analytis J, Xia Q, Asensio M and Wu J 2018 *Adv. Mater.* **30** 1800754
[21] Zhang J, Chen S, Du G, Yu Y, Han W, Xia Q, Jin K and Chen Y 2023 *Nano Lett.* **23** 8970
[22] Wang H, Zhong Y, Jiang W, Latini S, Xia S, Cui T, Li Z, Low T and Liu F 2024 *Nano Lett.* **24** 2057
[23] Zhong M, Meng H, Liu S, Yang H, Shen W, Hu C, Yang J, Ren Z, Li B, Liu Y, He J, Xia Q, Li J and Wei Z 2021 *ACS Nano* **15** 1701
[24] Geim A K and Grigorieva I V 2013 *Nature* **499** 419
[25] Liu Y, Stradins P and Wei S H 2016 *Sci. Adv.* **2** e1600069
[26] Farmanbar M and Brocks G 2016 *Adv. Electron. Mater.* **2** 1500405
[27] Novoselov K S, Fal'ko V I, Colombo L, Gellert P R, Schwab M G and Kim K 2012 *Nature* **490** 192
[28] Saeed M, Palacios P, Wei M D, Baskent E, Fan C Y, Uzlu B, Wang K T, Hemmetter A, Wang Z, Neumaier D, Lemme M C and Negra R 2022 *Adv. Mater.* **34** 2108437
[29] Hieu N N, Phuc H V, Ilyasov V V, Chien N D, Poklonski N A, Van Hieu N and Nguyen C V 2017 *J. Appl. Phys.* **122** 104301
[30] Liu Y, Rodrigues J N B, Luo Y Z, Li L, Carvalho A, Yang M, Laksono E, Lu J, Bao Y, Xu H, Tan S J R, Qiu Z, Sow C H, Feng Y P, Castro Neto A H, Adam S, Lu J and Loh K P 2018 *Nat. Nanotechnol.* **13** 828
[31] Padilha J E, Fazzio A and da Silva A J R 2015 *Phys. Rev. Lett.* **114** 066803
[32] Sun M L, Chou J P, Yu J and Tang W 2017 *Phys. Chem. Chem. Phys.* **19** 17324
[33] Yuan J, Wang F, Zhang Z, Song B, Yan S, Shang M H, Tong C and Zhou J 2023 *Phys. Rev. B* **108** 125404
[34] Binh N T T, Nguyen C Q, Vu T V and Nguyen C V 2021 *J. Phys. Chem. Lett.* **12** 3934
[35] Nguyen H T T, Obeid M M, Bafekry A, Idrees M, Vu T V, Phuc H V, Hieu N N, Hoa L T, Amin B and Nguyen C V 2020 *Phys. Rev. B* **102** 075414
[36] Cao L, Ang L Y S, Wu Q and Ang L K 2019 *Appl. Phys. Lett.* **115** 241601
[37] Liu Y, Qiu Z, Carvalho A, Bao Y, Xu H, Tan S J R, Liu W, Castro Neto A H, Loh K P and Lu J 2017 *Nano Lett.* **17** 1970
[38] Yang X, Sa B, Lin P, Xu C, Zhu Q, Zhan H and Sun Z 2020 *J. Phys. Chem. C* **124** 23699
[39] Mohanta M K, Arora A and De Sarkar A 2021 *Phys. Rev. B* **104** 165421
[40] Guo H, Lang X, Tian X, Jiang W and Wang G 2022 *Nanotechnology* **33** 425704
[41] Ebrahimi M R, Vazifehshenas T 2023 *Appl. Surf. Sci.* **616** 156489
[42] Feng X, Lan C S, Liang S J, Lee C H, Yang S A and Ang Y S 2024 *Adv. Func. Mater.* **34** 2309848
[43] Cao S, Li Z, Han J and Zhang Z 2024 *Surf. Interfaces* **46** 104022
[44] Gao Z, He X, Li W, He Y and Xiong K 2024 *Physica E* **155** 115837
[45] Liu X, Yang J, Deng X, Tang Z K and Cao L 2024 *ACS Appl. Electron. Mater.* **6** 2568
[46] Chen Z, Qiu H, Cheng X, Cui J, Jin Z, Tian D, Zhang X, Xu K, Liu R, Niu W, Qiu L, Chen Y, Zhang C, Xi X, Song F, Yu R, Zhai X, Jin B, Zhang R and Wang X 2024 *Nat. Commun.* **15** 2605
[47] Perdew J P, Burke K and Ernzerhof M 1996 *Phys. Rev. Lett.* **77** 3865
[48] Klimeš J, Bowler D R and Michaelides A 2011 *Phys. Rev. B* **83** 195131
[49] Bengtsson L 1999 *Phys. Rev. B* **59** 12301
[50] Van Troeye B, Lherbier A, Charlier J C and Gonze X 2018 *Phys. Rev. Mater.* **2** 074001
[51] Tung R T 2014 *Appl. Phys. Rev.* **1** 011304
[52] Bardeen J 1947 *Phys. Rev.* **71** 717
[53] Sanville E, Kenny S D, Smith R and Henkelman G 2007 *J. Comput. Chem.* **28** 899